Production of thin graphite sheets for a high electrical conductivity film by the mechanical delamination of ternary graphite intercalation compounds

Production of thin graphite sheets for a high electrical conductivity film by the mechanical delamination of ternary graphite intercalation compounds

Shinya Yamanaka, Tomoe Nishino, Toshiyuki Fujimoto, and Yoshikazu Kuga*

Department of Applied Sciences, Muroran Institute of Technology, Mizumoto-cho 27-1, Muroran 050-8585, Japan

*Corresponding author. Tel: +81 143 46 5747. Fax: +81 143 46 5701.

E-mail address: kuga@mmm.muroran-it.ac.jp (Y. Kuga)

Abstract:

Herein we propose a production scheme for conductive films composed of thin graphite sheets with high crystallinity and polymeric resin. The crystalline graphite sheets were successfully produced from natural graphite powder by solution-phase synthesis of graphite intercalation compounds (GICs), following a wet planetary-ball milling under mild conditions. The shear forces in the milling pot lead to a peeling of graphite flakes. Taking into consideration the interlayer bonding force, the delamination should be preferentially done from the expanded GICs interlayer rather than intrinsic graphite one. Some composite films derived from the phenolic resin and flaky graphite sheets displayed much higher electrical conductivities compared to the film from the feed graphite particles. We also demonstrate the stage structure of synthetic GICs affected the film conductivity. The composite films made from exfoliated products of ground (around stage IV) GICs exhibited high electrical conductivity with a small amount of the graphite sheets.

1. Introduction

Natural graphite is a cheap, abundant natural material, and has attracted great interest because of its excellent mechanical and chemical properties [1,2]. This makes it a promising raw material for versatile applications such as batteries [3], solar cells [4], and transparent conductive films [5,6]. Several investigations of polymer composite materials have been done focusing on particle size [7], aspect ratio [8] as well as the interaction with polymer matrix [9]. In these studies vapor-grown carbon fibers, carbon nanotubes, and thin graphite nano-sheets were often used as high-aspect filler. Recently, polymer composite materials have undergone an outstanding improvement in mechanical and electrical properties, while using a small amount of carbon fillers [5,8,10].

Highly crystalline natural graphite shows high electrical conductivity and excellent lubricant properties [11-13]. With these properties in mind, we have produced fine and flaky graphite particles, which exhibit high electrical conductivity, by grinding natural graphite particles under well-controlled milling atmospheres such as alcoholic vapor [14], nitrogen, hydrogen, oxygen, and vacuum [15]. Both the flaky shape of the graphite sheets and size reduction of the ground products with high crystallinity could be obtained in the milling process. There has been intensive research on finding new methods for the preparation of graphite sheets or even monolayer graphene sheets over the past few years.

Nevertheless, large-scale~~, economical~~ production of thin graphite sheets with high crystallinity remains challenging.

Two main processes are capable of producing thin graphite sheets (including graphene) so far. One is epitaxial growth on the substrate [16] and the other is large-scale exfoliation [17-19]. Liquid phase exfoliation is the most economical owing to low costs of manufacturing equipment and raw materials. Hernandez et al. [17] presented exfoliation of graphite by means of sonication in the organic solvent N-methyl-pyrrolidone. They have achieved a yield of monolayer graphene of up to 1 mass %. In addition, thin graphite nano-sheets have been produced by mechanical shearing in a comminuting mill. In this case, a surfactant or a dispersion agent is usually administered to prevent agglomeration and restacking of the delaminated sheets. More recently Peukert and his colleagues reported a scalable production scheme of ultrathin graphite sheets and graphene monolayers [19]. Mono- and multilayer graphene sheets assisted with a surfactant of sodium dodecylsulfate have been prepared in a stirred-media mill in mild milling conditions, yielding about 2.5 mass% at peeling times of only a few hours [19].

Herein we report a potentially scalable ~~and economical~~ production of highly crystalline graphite sheets by mechanical grinding of graphite intercalation compounds (GICs) without surfactant. After ternary GICs had been prepared, wet planetary ball milling

was performed to produce flaky graphite sheets with high crystallinity. Next, the flaky graphite sheets were mixed with a phenolic resin, and the resulting composite resin was coated onto a commercial glass slide to investigate the electrical conductivity. In this paper, we also demonstrate the influence of multi-stage GICs on the conductive properties of the composite resin.

2. Experimental procedure

2.1 Materials

Natural graphite (found in Brazil) with a mean particle size of 19.6 μm and a density of about 2.3 g/cm^3 was used as a starting material. The mean particle size, which corresponded to the 50 mass % diameter, was determined by using a laser diffraction particle size analyzer (MicroTrac MT3000EX, Nikkiso, Japan). Phenolic resin (nonvolatile content 43%, HD-2325) was purchased from DIC Kitanihon Polymer Co., Ltd. The feed natural graphite, potassium (assay 98%, Kishida Chemical Co., Ltd., Japan), tetrahydrofuran (purity>99.5%, Kanto Chemical Co., Inc., Japan), and naphthalene (purity>99%, Kanto Chemical Co., Inc., Japan) were used in GICs synthesis.

2.2 Preparation of thin graphite sheets

Schematic description of production of thin graphite sheets is given in **Fig. 1**. Thin graphite sheets were prepared by potassium–tetrahydrofuran–graphite ternary intercalation compounds (K–THF–GICs), followed by mild, wet, planetary-ball milling to apply a shear stress that leads to delamination of the GICs. The thickness of the graphite sheets was roughly controlled by the stage structure of K–THF–GICs. The delamination may occur in the intercalated layer because of the weak van der Waals interaction between expanded graphene sheets (0.88 nm [20]) rather than the intrinsic graphene sheets (0.335 nm). A delamination mechanism based on the interlayer structure will be described in section 3.1.

The subsequent treatment deals with the unnecessary organic solvent and the dissolved potassium. The suspension (including ground products of GICs) was washed with ethanol and water to eliminate the excess base. In this process the GICs decompose completely to the residue compounds.

In the production of graphite sheets, all sample preparation and transfer of samples to another flask or a milling pot were performed in the glovebox under argon atmosphere. (Saturated pressure of water vapor in the box was maintained below 191.4 Pa.).

First, K–THF–GICs were synthesized by using a liquid intercalation technique at room temperature using potassium and tetrahydrofuran [20]. Briefly, the feed natural graphite particles were immersed into a mixture of potassium, naphthalene, and 200 ml

THF. The solution was placed in a round-bottom flask under an argon atmosphere and stirred slowly in an argon gas flow of 0.1 *l*/min for 2 days. Synthesis conditions for various stage structures of K–THF–GICs are summarized in **Table 1**.

Next, the prepared K–THF–GICs were delaminated through a wet ball milling process. The grinding treatments were carried out in a planetary-ball mill (PM 100, Retsch, Germany) with a stainless steel pot of 500 cm^3 capacity and 100.5 mm inner diameter. The mixture with K–THF–GICs, used as the grinding stock, was sealed directly in the pot filled with 630 g of grinding media. The revolution speed of the pot was adjusted to 400 rpm. Commercially available yttria-stabilized zirconia beads with 300-μm diameter were used as the grinding media. According to the manufacturer (Nikkato Corporation, Osaka, Japan), the milling beads have a chemical composition of 95% zirconia and 5% yttria. After 4 hours of grinding, the suspension was diluted with ca. 100 ml of ethanol and ca. 1000 ml of purified water, neutralized with dilute hydrochloric acid solution and carefully rinsed with an adequate amount of purified water to remove the THF and any residue. It should be noted that moist graphite sheets were obtained in the collection process because it was quite difficult to redisperse the completely dry and agglomerated graphite sheets into the polymeric resin. The suspension was then filtered using filter paper (pore size 3 μm) in order to collect the moist sample of which the water content was ca. 80 mass%. Effect of

the collection process on colloidal stability of the graphite sheets into a polymer phase will be discussed in section 3.2.

The shapes of the graphite sheets were studied with scanning electron microscopy (SEM, JSM-6380A, JEOL). X-ray diffraction (XRD, MultiFlex, Rigaku) powder patterns of the samples were obtained with Cu Kα (wavelength λ=1.5418 Å) radiation (40 kV, 40 mA) to establish average crystallite size, was calculated using Scherrer's equation according to the literature [21]. ~~In this study, the mean stack height of the graphite crystallites, L_c, was obtained from the 002 diffraction peak.~~ In this study, carbon hexagonal plane (L_a) and the mean stack height (L_c) of the graphite crystallites were obtained from the 100 and 002 diffraction peak, respectively. The crystallite size was presented as averaged values based on five experimentally determined values.

2.3 Electrical conductivity measurement

The moist or completely dry graphite sheet was used as the starting material for graphite sheet-based phenolic composites. We added 6.0–50.0 mass% graphite sheets to 1.0 g phenolic resin, and the mixture was ground for 5 min in an agate mortar with a pestle. The resulting composite resin was coated onto a commercial glass slide, dried at 60°C for 1

hour, and heated to 130°C in 5 min in order to polymerize the resin. This method of preparing the composite resin is suitable for measuring electrical conductivity [22]. To investigate the electrical conductivity of the composite resin, the average resistance was measured at 10 sampling points by using two kinds of resistance instruments. A Loresta AP (for $<10^6$ Ω) and Hiresta UP (for $>10^6$ Ω) purchased from Mitsubishi Chemical Analytech Co., Ltd. were used. Specific resistance was calculated from the measured film resistance, *L*, and film thickness, *R*, as expressed in equation 1.

$$\rho = R \cdot F \cdot L \tag{1}$$

The film thickness, *L*, was obtained from the difference in average thickness between the glass slide and the coated glass. *F* is the correction coefficient, which was determined from the distance between the probes attached with the instruments. The values are 4.532 and 10.09 for the Loresta AP and for the Hiresta UP, respectively.

3. Results and discussion

3.1 Delamination of graphite sheets assisted with ternary GICs

In planetary ball milling, two routes to particle size reduction can be predicted: a shear

force leading to the peeling of thin sheets from the graphite surface or compressive normal forces leading to the breakage of the graphite flakes. ~~**Figure 2** shows SEM images of the feed natural graphite particles and several representative pictures of ground products. Initial graphite particles with their bulky stacking structure are shown in Fig. 2(a). When the feed natural graphite particles were ground into the THF solution, the particles were very similar in thickness (Fig. 2(b)). On the contrary, ground product prepared by stage IV K–THF–GIC in Fig. 2(c) revealed some exfoliated graphite interlayers and delamination of the graphite sheets. These observations suggest that a peeling of thin sheets assisted with K–THF–GICs is the more likely mechanism for size reduction.~~ **Figure 2** shows SEM images of the feed natural graphite particles and several representative pictures of ground products. These observations suggest that the flake structure remains after the grinding process without size reduction. Initial graphite particles with their bulky stacking structure are shown in Fig. 2(a). When the feed natural graphite particles were ground into the THF solution, the ground particles were very similar to the feed particles in shape (Fig. 2(b)). On the contrary, the feed graphite and its ground product had more bulky stacking structure compared to the ground product prepared by stage IV K–THF–GIC in Fig. 2(c).

Let us now focus on the effect of expanded interlayer on a delamination from graphite body, as shown schematically in **Fig. 3**. In order to explain the interlayer stability of the

present graphite sheets, it is useful to discuss the van der Waals interaction energy between the graphite sheets [19]. Because electrostatic interactions are negligible in such a relatively low dielectric constant medium [23] (dielectric constant of THF at 298 K is 7.58 [24]), we assume the van der Waals interlayer interactions were the main ones in the present system. Generally, van der Waals interaction energy per unit area, U_{vdW}, between two sheets of the thickness h_1 and h_2 with a separation distance d into a solvent can be described as follows [25].

$$U_{\mathrm{vdW}}(D) = -\frac{A}{12}\left(\frac{1}{d^2} + \frac{1}{(d+h_1+h_2)^2} - \frac{1}{(d+h_1)^2} - \frac{1}{(d+h_2)^2}\right) \tag{2}$$

where A (=6.4×10^{-20} J) is the Hamaker constant [23], calculated from the Hamaker constants of graphite particle (=2.38×10^{-19} J [26]) and THF (=5.55×10^{-20} J), A=(23.8$^{0.5}$–5.55$^{0.5}$)^2×10^{-20}. The Hamaker constant for THF A_{THF} was calculated according to the equation below [23].

$$A_{\mathrm{THF}} = 24\pi D_0^2 \gamma \tag{3}$$

In this equation γ is the surface tension (=27.04 mN/m at 298 K [27]), and the cutoff

distance D_0 is set to 0.165 nm [23]. Generally, surface tension of a solvation system changed slightly with pure solvent. For example, surface tension of 5 mass% potassium chloride solution at 298 K is 73.46 mN/m [28]. The difference in the surface tension was only ca. 1% compared to pure water (72.75 mN/m). In this study, potassium and naphthalene were dissolved in THF at the maximum concentration of 4.6 mass% (case stage I, see Table 1). We then assumed the effective Hamaker constant of THF dissolved potassium and naphthalene to be that of pure THF, since the two surface tensions were so similar.

Figure 4 demonstrates the van der Waals interaction energy per unit contact area as a function of the thickness of the delaminated sheet h_1. The distance d between the two sheets was chosen to be 0.335 nm for the interlayer separation of intrinsic graphite and 0.88 nm [20] for the K–THF–GICs. The thickness of another sheet h_2 was 19.6 μm, which corresponds to the mean size of the initial graphite particles. The required delamination energy for the intrinsic graphite interlayer and for the expanded one is about 15×10^{-3} and 2.2×10^{-3} J/m^2, respectively. The delamination of K–THF–GIC takes over 85% less energy than that of the feed natural graphite. This result clearly indicates that the expanded interlayer is energetically favorable to the delamination, i.e. the thickness of the graphite sheets in the milling pot is significantly affected by the stage structure of ternary GICs.

During the delamination in the ball milling, the graphite particles are under stress from the grinding media. The shear and compressive normal forces may lead not only to the generation of the delaminated sheets but also unwanted breakage of the carbon hexagonal planes as a basic unit common to graphitic materials. The creation of an amorphous graphite or a crystal-structural disorder in the carbon hexagonal plane should be avoided because this poorly-crystalline graphite would result in a decline of electrical conductivity [14,15]. We investigate the effect of the milling conditions, in particular, the small bead diameter of 300 μm, on the crystallinity of the grinding product. **Table 2** shows the crystallite size of grinding products by various stages of K–THF–GICs. The crystallite size of the ground graphite sheets was calculated from the full width at half maximum (FWHM) of the corrected diffraction profile. ~~A Pseudo-Voigt fitting was carried out to obtain the FWHM for the (002) diffraction, which represent the *c*-axis of the graphite hexagonal planes. The average crystallite size and its population standard deviation was calculated from five data points. In Table 2 we also present the crystallite size of the feed graphite particle and its ground product in THF. Although the ground products from feed graphite and the GICs experienced a slight decline in crystallite size (10±3–24.1±0.7 nm) compared with the initial feed graphite (34.0±0.3 nm), the present milling conditions make it possible to keep the crystallinity relatively high.~~ A pseudo-Voigt fitting was carried out to obtain the

FWHM for the (100) and (002) diffractions, which represent the *ab*-axis and *c*-axis of the graphite hexagonal planes. The average crystallite size and its population standard deviation were calculated from five data points. In Table 2 we also present the crystallite size of the feed graphite particles and its ground product in THF. The ground products from feed graphite and the GICs experienced a slight decline in crystallite size (10±3~21±1 nm for (100) and 10±3~24.1±0.7 nm for (002)) compared with the initial feed graphite (30±2 nm for (100) and 34.0±0.3 nm for (002)). The mild milling conditions, with small bead (300-μm diameter), produce a mechanical delamination of the GICs rather than compressive fractures. The wet grinding using a planetary ball mill with fine beads could minimize a transformation into amorphous graphite. We demonstrate that shear was the main force during the ball milling process, as expected, in Fig. 1.

3.2 Electrical conductivity of the composite resin

The specific resistance of the composite films was measured for several weight fractions of the filling graphite products. **Figure 5** shows the influence of the stage structures on the specific resistance of the films. The composite film made from graphite ground into THF had 10^1–10^2 higher resistance than the film filled with natural graphite at every weight fraction~~, indicating that the ground products were rather poor electrical~~

~~conductors (see Table 2)~~. The major cause of the poor conductivity at small mass fractions of the product ground in THF is the failure of feed graphite to delaminate. The calculated delamination energy (Fig. 4), calculated from the van der Waals interaction energy for the intrinsic graphite interlayer, could not reach delamination under these grinding conditions. The grinding in THF yielded particles similar in number to those of feed graphite. Consequently, these could not connect with each other to form conductive paths with small mass fractions. When feed graphite was ground into THF, its crystallinity was worse compared to the feed natural graphite (as can be seen in Table 2). Because poor crystallinity leads to low electrical conductivity [11], the ground products were rather poor electrical conductors. Except the ground feed graphite, however, composite films filled with the exfoliated products of grinding GICs clearly showed low specific resistance in comparison with the feed graphite. In particular, the composite filling the exfoliated product of grinding stage IV K–THF–GIC displayed low resistance even below 10 mass % fraction.

It should be noted that there is an optimal stage structure for obtaining a highly conductive film. This is due to the combined effects of the aspect ratio and crystallinity. Since the width-to-thickness aspect ratio of graphite sheets would be high on exfoliated products of grinding lower-stage GICs, they could connect with each other to form conductive paths with even small mass fractions. However, poor crystallinity leads to low

electrical conductivity [11], resulting in a poorer conductivity of the composite film. Kim et al. have pointed out the importance of the graphite crystallite to make high electrically conductive composites [29]. They synthesized composite films containing well-dispersed thin graphite sheets by in-situ polymerization and demonstrated that the film with the stage IV GIC exhibited the highest electrical conductivity between stages I and IV of GICs [28].

The most illustrative exposition of the structural dependency in the above measurement results is the plots (solid black square) in **Fig. 6**. The horizontal axis denotes the inverse of stage structure, representing the composite film using stage ∞ in the same figure. By infinity we denote the ground products of the feed natural graphite being milled into the THF solvent.

Specific resistances were measured when 10 mass % of the conductive material was added. The specific resistance for the composite film including the feed graphite was 10^7 Ω·cm. When the number of percolated graphite sheets increases, the specific resistance decreases, reaching ca. 10^1 Ω·cm for the composite filled with the exfoliated products of grinding stage III or IV K–THF–GIC. A mild increase in the specific resistance of 10^3 Ω·cm was observed with respect to composite of the stage I K–THF–GIC.

Now we discuss the redispersibility of prepared graphite sheets during the collection and the film preparation process. The agglomeration or restacking of the peeling sheets

reduces the apparent particle number density, which has an enormous impact on the film resistance. We have not used any surfactants or dispersants in the present study because we focused on the stage structure of K–THF–GICs. Since surfactants can become intercalants [30], their introduction would make it more complex and difficult to control the stage structure of the graphitic materials.

Another experiment was performed to point out the importance of the redispersibility into the polymeric matrix. The difference in the specific resistance of films between the moist and the dried graphite sheets was estimated. The completely dried graphite sheets were mixed with phenolic resin, and the composite films were similarly prepared as described in section 2.3. Their specific resistances are also plotted (open squares) in Fig. 6. Phenolic resin contains 57 mass% volatile organic contents. Note that weight loss of the films at 373 K, both for films prepared from moist and dried samples, determined by thermogravimetric-differential thermal analysis (TG-DTA; Seiko Instruments Exstar 6200N, 50 m*l*/min nitrogen flow, 10 K/min ramp) was 8.4±2.9 mass% and 8.3±2.9 mass%, respectively. **Figure 7** shows the DTG curves of the composite films prepared from moist and dried samples. The two curves have very similar peaks at ca. 348 K. These findings indicate a large amount of volatile contents, though little water was contained in the films. Consequently, we do not believe that water had any influence on the electric conductivity

of the phenolic resin films. The films composed of the completely dried sheets still had lower resistance than the feed natural graphite. Moist sheets, however, had electrical conductivities that were especially prominent in the lower stage samples (stages I, III, and IV). The dried sheet by stages I, III, and IV had specific resistance 10^3, 10^2, and 10^1 times larger, respectively, than the moist one. This finding gives qualitative evidence of agglomeration and restacking of the delaminated sheets into the phenolic resin.

A surfactant is needed to prevent agglomeration and restacking of the delaminated sheets. Sodium dodecylsulfate [19,30], sodium deoxycholate [31,32], TritonX [33,34], and etc. were commonly used as surfactants that adsorb onto the carbon-based particle resulting in strong repulsive forces. The method proposed in this research, whereby the wet graphite sheets were simply mixed with the phenolic resin, can result in highly conductive resin, by adding a small amount of graphite sheets in the absence of surfactant, although the method is still in its infancy. In the present study, we could not show the dispersion state of graphite sheets into the composite films in detail. Instead, by measuring the specific resistance of the films, we showed whether the conductive path was formed or not, as well as whether or not the sheets were connected to each other in the resin. These macroscopic findings are an important step toward practical use. The effect of a surfactant on the dispersibility of the flaky graphite into the phenolic resin will be investigated in the near future. It should be

emphasized that mechanical delamination from ternary GICs is a realistic production technique for several-layer-thick graphite sheets with high crystallinity. This method can achieve 50 g/L (over 5 mass%) per batch of thin graphite sheets. K–THF–GIC is highly unstable under ambient air conditions. Therefore, all sample preparation and transfer of samples to another flask or a milling pot were performed in a glovebox under argon atmosphere, as mentioned in section 2.2. One of the features of this process is that the mixture including solvent and K–THF–GICs was sealed directly in the pot, and ground without air exposure. We then obtained flaky graphite particles after ground product of K–THF–GICs was carefully rinsed with ethanol and an adequate amount of purified water to remove THF and any residues. Because these are stable graphite particles, we can treat them under ambient air conditions. We believe that many comminuting processes using small beads should be applicable to the delamination of expanded layered materials.

4. Conclusions

High-crystallinity, thin graphite sheets were produced by mechanical delamination of the ternary GICs. The two actions: the wet planetary ball milling with small beads and the expanded interlayer of GICs, are effective in overcoming the van der Waals forces between the expanded graphene sheets that prevent the excess breakage of the carbon hexagonal

plane. We have also demonstrated that the specific resistance of the composite films was greatly affected by the stage structure of the synthetic ternary GICs. There is an optimal stage structure of the GICs for obtaining highly conductive films. Specifically, the composite filling the exfoliated products of grinding stages III and IV K–THF–GIC displayed the lowest resistance at 10 mass % of the weight fraction. The scheme proposed in this study is ~~an economical and~~ a scalable production of thin graphite sheets as the starting material for composite resins with highly conductivity.

References

[1] Shim JP, Striebel KA. Cycling performance of low-cost lithium ion batteries with natural graphite and $LiFePO_4$. J Power Sources 2003;119-121:955-8.

[2] Ubrig N, Plochocka P, Kossacki P, Orlita M, Maude DK, Portugall O, et al. High-field magnetotransmission investigation of natural graphite. Phys Rev B 2011;83(7):073401.1-4.

[3] Zhang HL, Liu SH, Li F, Bai S, Liu C, Tan J, et al. Electrochemical performance of pyrolytic carbon-coated natural graphite spheres. Carbon 2006;44(11):2212-8.

[4] Hsieh CT, Yang BH, Lin JY. One- and two-dimensional carbon nanomaterials as counter electrodes for dye-sensitized solar cells. Carbon 2011;49(9):3092-7.

[5] Stankovich S, Dikin DA, Dommett GHB, Kohlhaas KM, Zimney EJ, Stach EA, et al. Graphene-based composite materials. Nature 2006;442(7100):282-6.

[6] Liu Z, Guo Q, Shi J, Zhai G, Liu L. Graphite blocks with high thermal conductivity derived from natural graphite flake. Carbon 2008;46(3):414-21.

[7] Nagata K, Iwabuki H, Nigo H. Effect of particle size of graphites on electrical conductivity of graphite/polymer composite. Compos Interfaces 1998;6(5):483-95.

[8] Al-Saleh MH, Sundararaj U. A review of vapor grown carbon nanofiber/polymer conductive composites. Carbon 2009;47(1):2-22.

[9] Wu G, Miura T, Asai S, Sumita M. Carbon black-loading induced phase fluctuations in PVDF/PMMA miscible blends: dynamic percolation measurements. Polymer 2001;42(7):3271-9.

[10] Chen G, Wu D, Weng W, Wu C. Exfoliation of graphite flake and its nanocomposites. Carbon 2003;41(3):619-21.

[11] Kuga Y, Oyama T, Wakabayashi T, Chiyoda H, Takeuchi K. Laser-assisted exfoliation of potassium-ammonia-graphite intercalation compounds. Carbon 1993;31(1):201-4.

[12] Kuga Y, Endoh S, Oyama T, Chiyoda H, Takeuchi K. Effect of exfoliation ratio on the flakiness of fine graphite particles obtained by grinding of exfoliated graphite. Carbon 1997; 35(12):1833-6.

[13] Kuga Y, Endoh S, Chiyoda H, Takeuchi K. Grinding characteristics of bromine-exfoliated graphite and natural graphite. Powder Technol 1990;60(2):191−6.

[14] Kuga Y, Shirahige M, Fujimoto T, Ohira Y, Ueda A. Production of natural graphite particles with high electrical conductivity by grinding in alcoholic vapors. Carbon 2004;42(2):293-300.

[15] Kuga Y, Shirahige M, Ohira Y, Ando K. Production of finely ground natural graphite particles with high electrical conductivity by controlling the grinding atmosphere. Carbon 2002;40(5):695-701.

[16] Berger C, Song ZM, Li XB, Wu XS, Brown N, Naud C, et al. Electronic confinement and coherence in patterned epitaxial graphene. Science 2006;312(5777):1191-6.

[17] Hernandez Y, Nicolosi V, Lotya M, Blighe FM, Sun Z, De S, et al. High-yield production of graphene by liquid-phase exfoliation of graphite. Nat Nanotechnology 2008;3(9):563-8.

[18] Shih CJ, Vijayaraghavan A, Krishnan R, Sharma R, Han JH, Ham MH, et al., Bi- and trilayer graphene solutions. Nat Nanotechnology 2011;6(7):439-45.

[19] Knieke C, Berger A, Voigt M, Taylor RNK, Rohrl J, Peukert W. Scalable production of graphene sheets by mechanical delamination. Carbon 2010;48(11):3196-204.

[20] Tanaike O, Inagaki M. Ternary intercalation compounds of carbon materials having a low graphitization degree with alkali metals. Carbon 1997;35(6):831-6.

[21] Iwashita N., Park CR, Fujimoto H, Shiraishi M, Inagaki M. Specification for a standard procedure of X-ray diffraction measurements on carbon materials. Carbon 2004;42(4):701-14.

[22] Hirabayashi Y, Nishino T, Fujiwara Y, Fujimoto T, Kuga Y. Production of flaky graphite particles by the exfoliation method and their application to electrical conductive composite films (in Japanese). J Soc Powder Technol, Japan 2010;47(10):684-91

[23] Israelachvili JN. Intermolecular and surfaces forces (2nd edn.). London: Academic Press;1992.

[24] Covington AK, Dickinson T. Physical chemistry of organic solvent systems. New York : Plenum;1973.

[25] Tadmor R. The London-van der Waals interaction energy between objects of various geometries. J Phys Condens Matter 2001;13(9):L195-202.

[26] Dryzmala J. Hydrophobicity and collectorless flotation of inorganic materials. Adv Colloid Interface Sci 1994;50(1-3):143-85.

[27] Pan C, Ouyang G, Yang Y, Zhen X, Huang Z. Excess molar volumes and surface tensions of trimethylbenzene with tetrahydrofuran tetrachloromethane and dimethyl sulfoxide at 298.15K. J Chem Eng Data 2004;49(6):1839-42.

[28] Yamada M, Fukusako S, Kawanami T, Sawada I, Horibe A. Surface Tension of Aqueous Binary Solutions. Int J Thermophys 1997; 18(6):1483-93.

[29] Kim H, Hahn HT, Viculis LM, Gilje S, Kaner RB. Electrical conductivity of graphite/polystyrene composites made from potassium intercalated graphite. Carbon 2007;45(7):1578-82.

[30] Alanyalioglu M, Segura JJ, Oro-Sole J, Casan-Pastor N. The synthesis of graphene sheets with controlled thickness and order using surfactant-assisted electrochemical

processes. Carbon 2012;50(1):142-152.

[31] Xu H, Abe H, Naito M, Fukumori Y, Ichikawa H, Endoh S, et al. Efficient dispersing and shortening of super-growth carbon nanotubes by ultrasonic treatment with ceramic balls and surfactants. Adv Powder Technol 2010;21(5):551-5.

[32] Moriarty GP, Wheeler JN, Yu C, Grunlan JC. Increasing the thermoelectric power factor of polymer composites using a semiconducting stabilizer for carbon nanotubes. Carbon 2012;50(3):885-95.

[33] Erdinç N, Göktürk S, Tunçay M. A study on the adsorption characteristics of an amphiphilic phenothiazine drug on activated charcoal in the presence of surfactants. Colloids Surf B: Biointerfaces 2010;75(1):194-203.

[34] Majumder M, Rendall C, Li M, Behabtu N, Eukel JA, Hauge RH, et al. Insights into the physics of spray coating of SWNT films. Chem Eng Sci 2010;65(6): 2000-8.

Table(s)

Table 1. Weight ratios for different stage of potassium–tetrahydrofuran–graphite intercalation compounds (K–THF–GICs).

Stage	Graphite (g)	Potassium (g)	Naphthalene (g)
I	10.0	4.26	4.26
III	10.0	0.86	0.86
IV	10.0	0.67	0.64
VI	10.0	0.46	0.47
X	10.0	0.25	0.29

Table 2. Crystallite sizes, L_a and L_c, of the feed natural graphite and ground products.

Stage	I	III	IV	VI	X	∞ [a)]	Feed [b)]
L_a(100) (nm) [c)]	10±3	15±2	16±6	18±3	17±3	21.2±1.1	30±2
L_c(002) (nm) [c)]	10±3	15±2	18±3	20±2	19.7±0.8	24.1±0.7	34.0±0.3

a) The ground product obtained by wet ball milling of the feed natural graphite in THF.

b) Initial natural graphite.

c) Average crystallite size and its population standard deviation is obtained from 5 data points.

Figure(s)

Figures

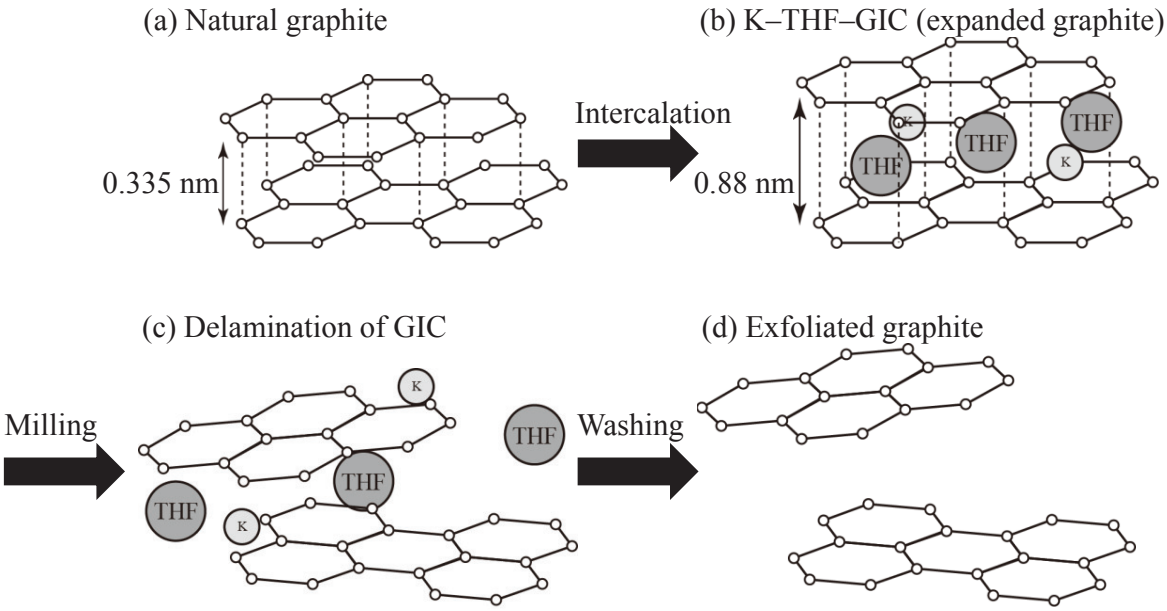

Figure 1. Production scheme of thin graphite. Natural graphite (a) is intercalated to prepare thin graphite sheets via potassium–tetrahydrofuran–graphite ternary intercalation compounds (K–THF–GICs) (b), followed by mild, wet, planetary-ball milling. The milling applies a shear stress that leads to the delamination of the GICs (c). Finally, the delaminated GICs are washed to obtain exfoliated graphite sheets (d).

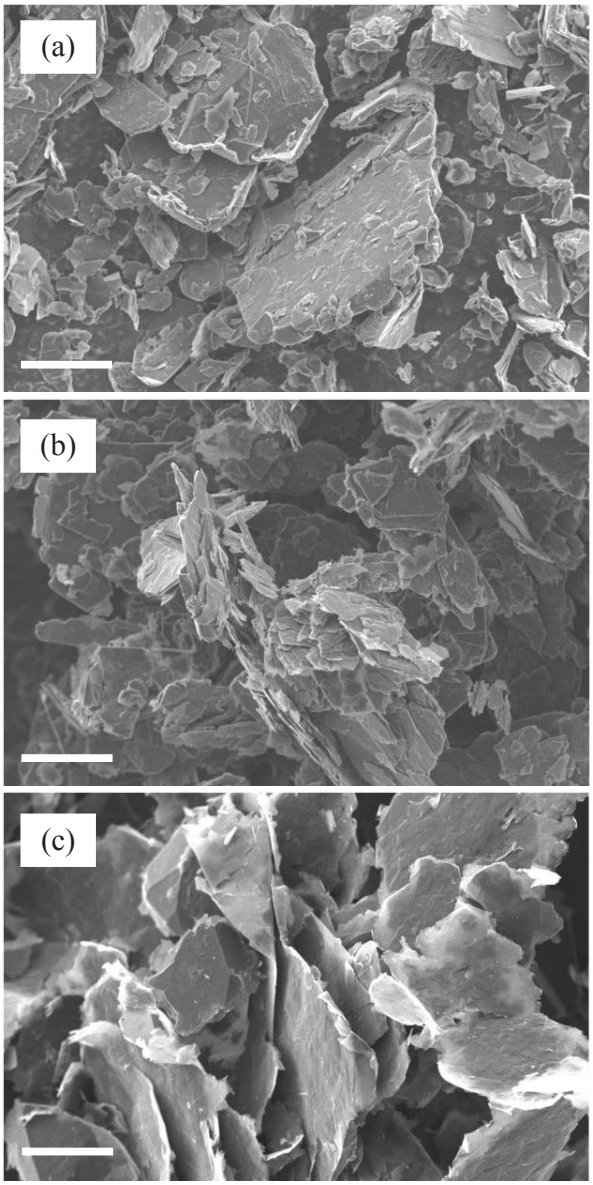

Figure 2. Typical images of the feed graphite particles and their ground products. (a) Feed natural graphite particles, (b) Ground products of the feed graphite into THF, and (c) Exfoliated products of grinding stage IV K–THF–GIC. The scale bar is 20 μm.

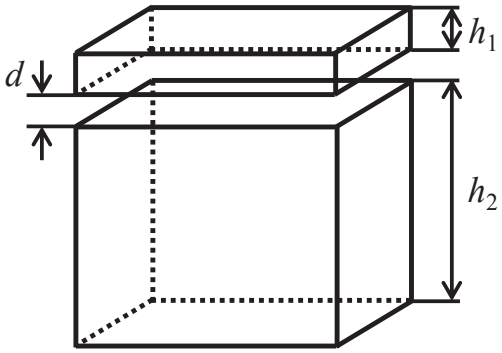

Figure 3. Schematic representation of a model used to investigate the peeling of graphite sheets. Graphite particle of thickness h_2 and delaminated thin graphite sheet of thickness h_1 are separated by a surface-to-surface distance d.

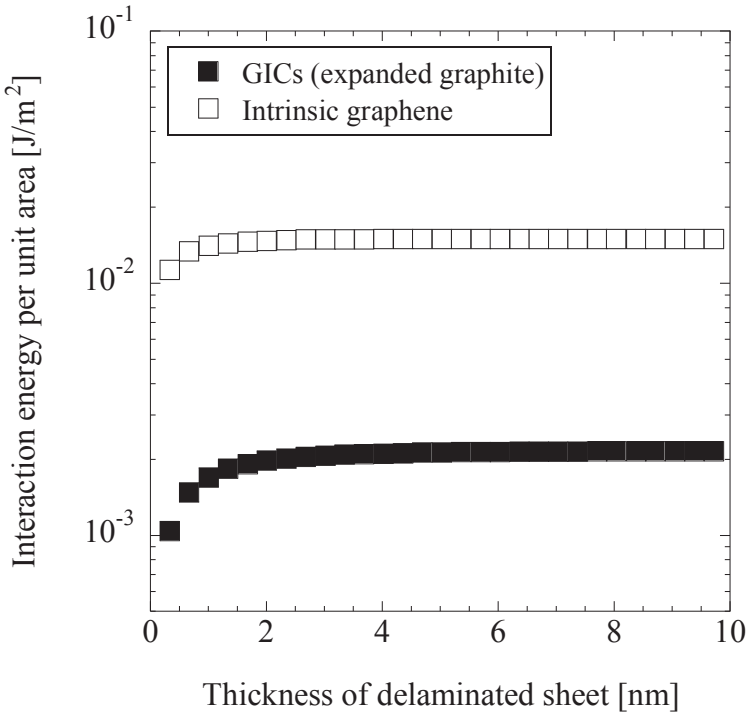

Figure 4. Interaction energies per unit area between two plates of finite thickness.

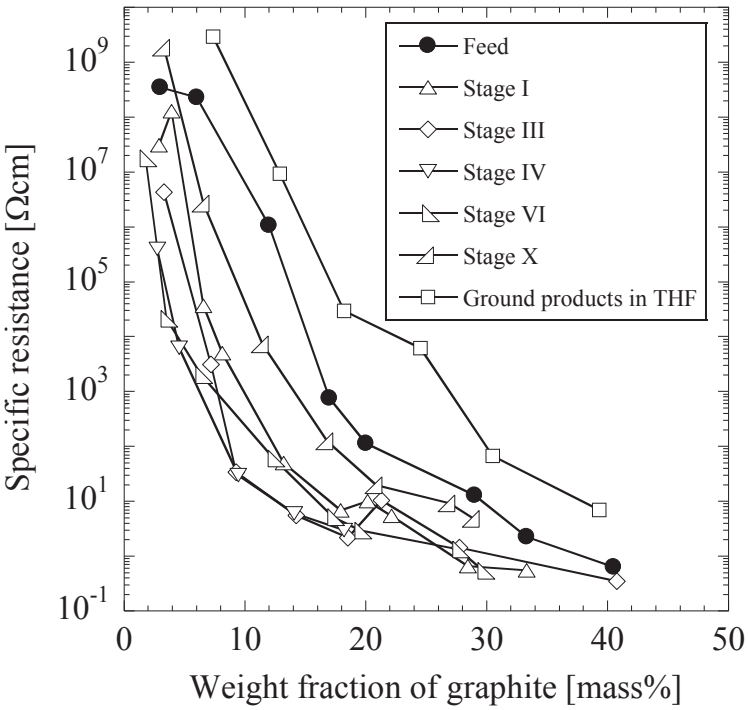

Figure 5. The relation between the weight fraction of graphite and the specific resistance of composite film consisting of several stage structures.

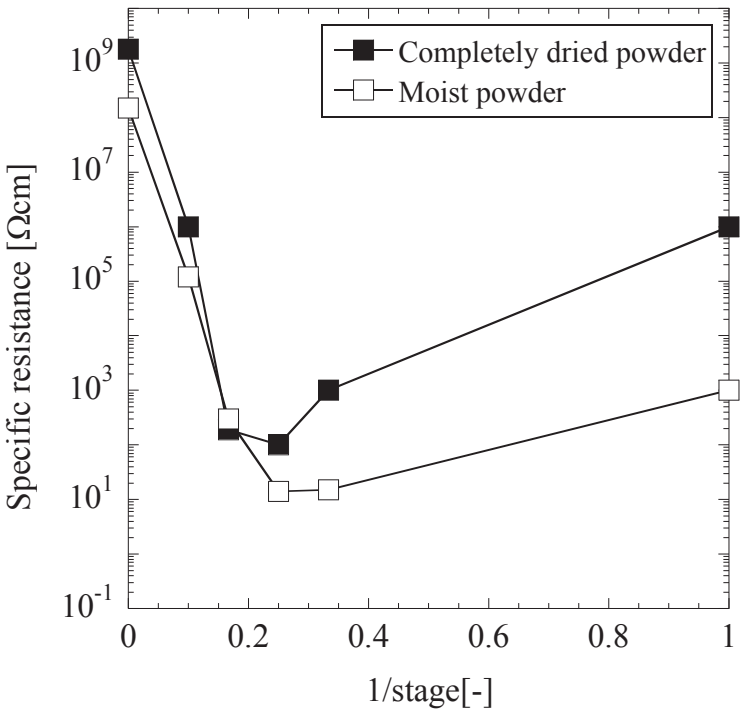

Figure 6. Structural dependency of the estimated specific resistance at 10 mass % of the filled graphite.

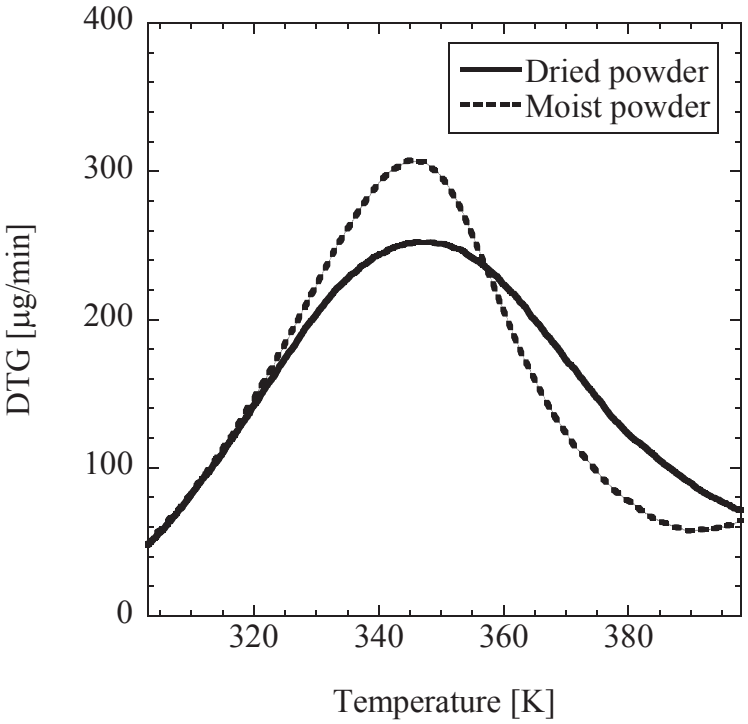

Figure 7. Typical DTG curves for composite films prepared from moist and dried samples.